AIMS Environmental Science

AIMS Environmental Science, 11(1): 90–106.
DOI: 10.3934/environsci.2024006
Received: 23 November 2023
Revised: 03 January 2024
Accepted: 28 February 2024
Published: 06 March 2024

http://www.aimspress.com/journal/environmental

Research article

Sustainable plastic bottle recycling: employing zinc-deposited SBA-15 as a catalyst for glycolysis of polyethylene terephthalate

Pailin Srisuratsiri[1], Ketsarin Chantarasunthon[1], Wanutsanun Sudsai[1], Pichet Sukprasert[1], Laksamee Chaicharoenwimolkul Chuaitammakit[2,*] and Wissawat Sakulsaknimitr[1,*]

[1] Department of Fundamental Science and Physical Education, Faculty of Science at Sriracha, Kasetsart University, Sriracha campus, Chonburi 20230, Thailand
[2] Chemistry and Applied Chemistry, Faculty of Science and Technology, Suratthani Rajabhat University, 272 Moo 9, Surat-Nasan Road, Khuntale, Muang, Surat Thani 84100, Thailand

*** Correspondence:** Email: wissawat.s@ku.th, laksamee.cha@sru.ac.th.

Abstract: Novel catalysts for recycling PET bottles into monomers have been developed by depositing zinc onto the surface of SBA-15, mitigating ZnO catalyst agglomeration in glycolysis separation processes to enhance reaction yields. Various zinc compounds ($Zn(OAc)_2$, $ZnCl_2$, and $ZnSO_4$) were employed as substrates for catalyst design on the porous, high-surface-area material SBA-15 *via* impregnation. The presence of distinct Zn species on SBA-15 was confirmed through XRD and EDS analyses. The acidity of the catalyst, a crucial factor in the PET glycolysis process, was assessed using different Zn-containing precursors. NH_3-TPD measurement has revealed the highest acidity in $ZnCl_2$, followed by $Zn(OAc)_2$ and $ZnSO_4$, respectively. Glycolysis reactions with a PET:EG ratio of 1:5 and a 1% catalyst at 200°C for 2 hours revealed the catalytic efficacy of zinc-deposited compounds in the sequence $ZnCl_2$ > $Zn(OAc)_2$ > $ZnSO_4$. Surprisingly, the $ZnCl_2$ catalyst produced the highest yield of *bis*-2-hydroxyethyl terephthalate (BHET) at 75% and displayed exceptional recycling capability over three cycles, contributing significantly to resource recovery objectives aligned with the Sustainable Development Goals (SDGs).

Keywords: sustainable development goals; glycolysis; SBA-15; Zn catalyst; polyethylene terephthalate

1. Introduction

Polyethylene terephthalate (PET) is widely used for beverage packaging due to its exceptional properties, including transparency, gas and water resistance, high impact strength, UV resistance, and being lightweight. However, the global production and use of PET bottles have led to significant plastic waste, causing environmental pollution and reducing landfill space. Incineration as a waste management method not only generates energy but also contributes to air pollution. The Great Pacific Garbage Patch serves as a clear example of the negative impacts of plastic waste on a global scale, breaking down into microplastics that contaminate soil, water, and air. Studies have even found microplastics in seafood and human blood, which have been linked to respiratory problems and the development of cancer [1]. Additionally, the production of PET bottles relies on fossil fuels, contributing to greenhouse gas emissions and climate change. Therefore, immediate action is essential to address and prevent this issue from escalating into a worldwide public health and environmental crisis.

Recycling is a promising way to reduce waste in landfills. Various methods can be employed to recover PET, including primary (re-extrusion), secondary (mechanical), tertiary (chemical), and quadruple (energy recovery) methods that possess their own advantages and disadvantages in terms of cost, quality, and environmental impact. For primary and secondary methods, the properties of recycled-grade PET deteriorate by thermal degradation during the process due to contamination of acid, water, color, and additives in the plastic [2]. Chemical recycling, on the other hand, involves breaking down polymer chains into monomers, providing valuable feedstock for the plastic industry, and promoting a circular economy. Among the chemical recycling reactions, glycolysis has gained significant attention due to its moderate operating temperature, mild reagents, normal pressure, high yield, and scalability. Glycolysis involves the trans-esterification of PET polymers using glycols, primarily ethylene glycol (EG), resulting in the cleavage of ester linkages to obtain *bis*-2-hydroxyethyl terephthalate (BHET) [3].

However, without a catalyst, the glycolysis of PET is inherently slow. This is primarily because the adjacent aromatic ring in the PET structure stabilizes the carbonyl group, which has a low degree of reactivity. Zinc acetate ($Zn(OAc)_2$) is widely used as a catalyst in PET glycolysis, offering a high yield of BHET compared to other metal salts. Nevertheless, its drawback lies in the dissolution of the metal salt in EG, making it challenging to recover for reuse. Even trace amounts of metal ions remaining in the BHET monomer can adversely affect the properties of the polymer, including rheological behavior, discoloration, and degradation of polymer chains [2,4].

While solid catalysts composed of metal oxide particles, mostly transition metals, have been used, their toxicity poses significant risks to the environment. Zinc oxide (ZnO), a non-toxic metal oxide commonly found in sunscreen [5], presents a promising alternative. It is not only environmentally friendly, but also exhibits excellent catalytic potential. Previous studies have investigated the reactivity of ZnO in PET glycolysis, showing a high yield of BHET but requiring high operating temperatures and pressures (260 °C and 5 atm) [6]. Our work explored the use of ZnO nanoparticles via reflux under normal pressure to achieve a high yield of BHET [7], although the

aggregation of nanoparticles after use reduces the efficiency of the reaction acceleration. Furthermore, nanoparticles may mix with the wastewater used for BHET washing, potentially leading to environmental contamination that could impact living organisms. To address this issue, distributing the catalyst on the surface of a support material could be offered.

Santa Barbara Amorphous-15 (SBA-15) is a mesoporous silica with a uniform hexagonal pore, a narrow pore-size distribution, and a high surface area. It has been applied to be a supported material for ZnO to utilize in various applications, including photocatalytic degradation [8,9], antibacterial agents [10], and catalysts [11–13]. For instance, Bhuyan *et al.* successfully prepared a ZnO/SBA-15 catalyst for the synthesis of dihydropyrimidinones. The catalytic efficiency of the ZnO nanocomposite was superior to that of pure ZnO nanoparticles, requiring a lower catalyst loading and a shorter reaction time [11]. Yao *et al.* employed ZnO/SBA-15 for the glycolysis of PET, achieving a remarkable 91% yield of BHET. The authors also noted that the resulting product exhibited improved whiteness compared to catalysts such as $Zn(OAc)_2$, ZnO, and ionic liquids [14].

The role of zinc in the glycolysis reaction was studied and generally proposed at the acid site of the catalyst. Both zinc atoms and zinc ions (Zn^{2+}) possess the ability to activate the carbonyl group of PET, facilitating its reaction with EG. However, most of the solid catalysts described in the literature for the glycolysis of PET are composed of metals or metal oxides. In a notable study, Datta and Pasha reported the preparation of $ZnCl_2$ absorbed on silica for the synthesis of 4-methylcoumarins. Their results demonstrated that Zn^{2+} ions on the silica surface could catalyze the reaction and be reused up to five times without a significant loss in efficiency [15].

The objective of this research is to develop catalysts comprising Zn^{2+} ions and ZnO distributed on SBA-15 for the purpose of catalyzing the glycolysis of PET waste bottles. Metal salts, namely $Zn(OAc)_2$, $ZnCl_2$, and $ZnSO_4$, were introduced using a wet impregnation technique. The calcination temperature was maintained at a constant 550°C to prevent any alterations to the pore structure caused by excessive heat [10]. At this temperature, the Zn salts decompose in different ways, resulting in the formation of either ZnO or Zn^{2+} ions on the SBA-15 support material [16,17]. Subsequently, the prepared catalysts underwent characterization and were employed in the glycolysis of PET to investigate their efficiency and optimize reaction conditions.

2. Materials and methods

2.1. Materialss

The disposal PET bottles were collected, removed labels, and cleaned with detergent, then air-dried and cut into chips (size 0.3 × 0.3 cm), avoiding the adhesive area. The chips were pulverized using a rotary cutter to obtain a PET particle size of 0.1 mm, further dried at 60 °C in an oven to remove moisture, and stored in a zip bag. Pluronic P123 (copolymer), tetraethyl orthosilicate (TEOS), 37% w/w hydrochloric acid (HCl), zinc acetate ($Zn(OAc)_2$), zinc chloride ($ZnCl_2$), zinc sulfate ($ZnSO_4$), 95% ethanol, and ethylene glycol (EG) were analytical grade and used as received.

2.2. Synthesis of SBA-15

A Pluronic P123 solution was prepared by adding 4.0 g of Pluronic P123, 90.0 g of distilled water, and 60.0 g of 4 M HCl in a round-bottom flask. The mixture was stirred at room temperature for 2 hours until it was fully dissolved. Then, 8.5 g of TEOS was gradually added dropwise to the mixture while continuously stirring at 40 °C for 20 hours. The mixture was poured into the autoclave with the temperature controlled at 100 °C for 24 hours in an oven. After finishing the reaction, the autoclave was cooled to room temperature by soaking in water. The precipitate was filtered using vacuum filtration, washed thoroughly with 95% ethanol to remove the copolymer, and oven-dried at 100 °C for 24 hours. The resulting solid was calcine at 550 °C with a heating rate of 10 °C/min for 6 hours to obtain a white solid of SBA-15.

2.3. Synthesis of Zn/SBA-15

SBA-15 was added to the solutions of $Zn(OAc)_2$, $ZnCl_2$, or $ZnSO_4$ by controlling the concentration of Zn at 10% wt. The mixture was impregnated at room temperature for 7 days. The precipitate was filtered using vacuum filtration, washed with distilled water, and dried at 100 °C for 24 hours. The resulting solid was calcine at 550 °C with a heating rate of 10 °C/min for 6 hours to obtain the expected Zn^{2+} or ZnO distributed on SBA-15 support. The prepared catalysts doped by $Zn(OAc)_2$, $ZnCl_2$, and $ZnSO_4$ were designated as **ZA**, **ZC,** and **ZS**, respectively.

2.4. Glycolysis of PET plastics

PET particles were mixed with EG at a weight ratio of 1:5 in a digestion tube. The catalysts, calculated as a percentage of the weight of PET, were then added, and the mixture was heated in a digestion box for a specified period. The obtained mixture was filtered using the Büchner funnel and washed with hot distilled water to separate the catalyst and incomplete depolymerized PET. Distilled water was added to the filtrate and stirred using a magnetic bar for 45 minutes to dissolve EG from the product. Then, water was removed using a rotary vacuum evaporator until the volume of the remaining mixture was about 60 cm^3. The mixture was transferred to a conical flask, closed with parafilm, and then placed in a refrigerator (4 °C) for 24 hours to crystallize BHET. The white solid of BHET was filtered using a Büchner funnel and washed with cold distilled water several times. The product was placed in an oven at 60 °C for 24 hours. The weight of BHET was recorded for calculating the percent yield of BHET ($\%Y_{BHET}$) as in the equation below.

$$\%Y_{BHET} = \frac{\text{mol BHET}}{\text{mol PET}} \times 100$$

Where mol BHET is the weight of BHET divided by a molecular weight of BHET (254 g/mol) and mol PET is the weight of PET divided by a molecular weight of the repeating unit of PET (192 g/mol).

2.5. Characterization

The prepared catalysts were characterized by X-ray diffraction (XRD) (Rigaku, smart lab) to obtain the crystal information of the catalysts. Surface morphology and 2D projection pictures were examined by a field emission scanning electron microscope (SEM-Hitachi; SU-8030) equipped with Energy-dispersive X-ray spectroscopy (EDS) to determine the percentage of elements on the surface. A transmission electron microscope (TEM-Hitachi HT7700) was applied to explore the pore structure of SBA-15 and the lattice fringe of the Zn catalyst on the surface. Surface area, pore volume, and pore diameter were examined by the physisorption of N_2 molecules using a BET analyzer (Micromeritics, 3Flex). The chemical functional group was confirmed using Fourier transform infrared spectroscopy (Jasco; FT-IR4000). The chemical state information from the surface of the catalysts was revealed by X-ray photoelectron spectroscopy (AXIS Ultra DLD). Temperature-programmed desorption (NH_3-TPD) experiments on the catalysts were carried out using a TA instrument (SDT2960 Simultaneous DTA-TGA Universal 2000). Differential scanning calorimetry (DSC, Netzsch DSC 214 polyma) was applied to confirm the purity of BHET products.

3. Results and Discussion

3.1. Characterization of the catalysts

3.1.1. Chemical structure

The XRD spectra of the samples reveal intriguing findings. Figure 1 presents a broad peak within the 15-40 2-theta range, indicating the presence of amorphous silica. The distinctive peak pattern of ZnO wurtzite was observed in the **ZA** within the 2-theta range of 30-70. The signals of the **ZS** spectrum correspond to the crystalline structure of $ZnSO_4 \circ H_2O$ [pdf card No: 01-074-1331], indicating the unchanged nature of the $ZnSO_4$ precursor. These observations can be attributed to the different decomposition temperatures of the various zinc salts, where $Zn(OAc)_2$ decomposed at 280°C, $ZnCl_2$ at 500°C, and $ZnSO_4$ at 680°C, respectively [11,13]. Consequently, the experimental calcination temperature set at 500°C was exclusively adequate for the transformation of $Zn(OAc)_2$ to ZnO. Nonetheless, the applied temperature might have been sufficient for **ZC** transformation, but the heating time possibly fell short of completely decomposing $ZnCl_2$ into ZnO. Accordingly, it is plausible that the size of the ZnO crystallites was too small to be detected by the XRD technique. As for **ZC**, the applied temperature might have been sufficient, but the heating time possibly fell short of completely decomposing $ZnCl_2$ into ZnO. Consequently, it is plausible that the size of the ZnO crystallites was too small to be detected by the XRD technique [10,18].

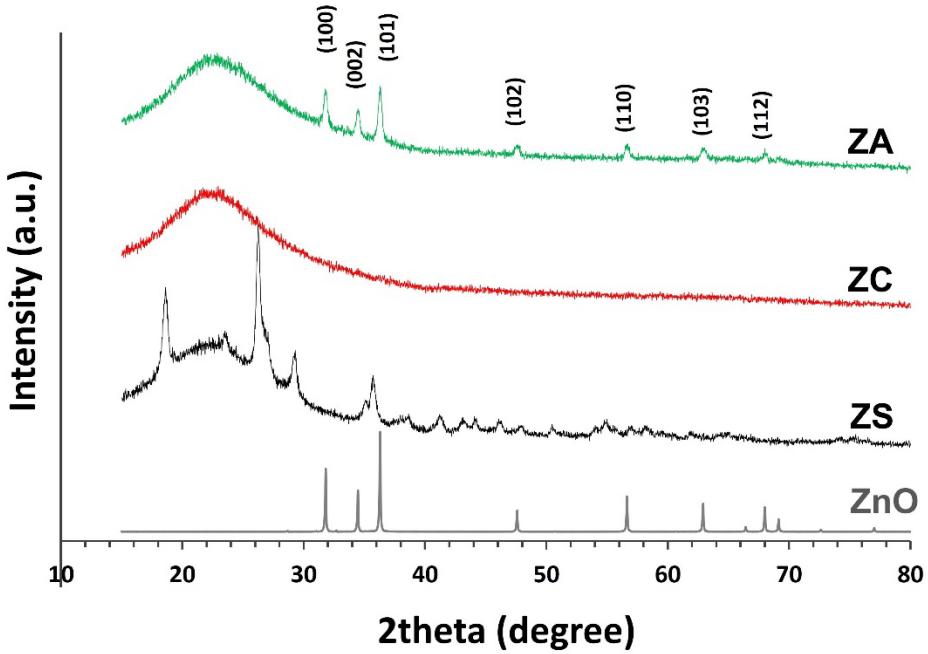

Figure 1. XRD patterns of the catalysts, prepared by impregnation and calcination at 550 ℃.

Figure 2 displays the FTIR spectra of all the samples. The weak broad peaks at wavenumbers 3454 cm^{-1} (stretching and bending vibrations in the O−H bonds of silanol groups (Si−O−H)) and 1639 cm^{-1} suggest the residual adsorbed water molecules [19]. The relatively weak intensity of the O−H signal indicates a low level of O−H functionality on the surfaces of the samples. Notably, a strong broad peak within the range of 1280-1000 cm^{-1} and a weak peak at 800 cm^{-1} correspond to the asymmetric and symmetric stretching vibrations of Si−O−Si, and the prominent signal at 460 cm^{-1} pertains to the bending vibration of Si−O−Si, respectively. Additionally, a minor peak at 965 cm^{-1} was attributed to the asymmetric stretching of Si-OH [20]. Surprisingly, the characteristic ZnO signal at 400 cm^{-1} disappeared for the catalyst samples, indicating a limited presence of the catalyst on the surface of SBA-15.

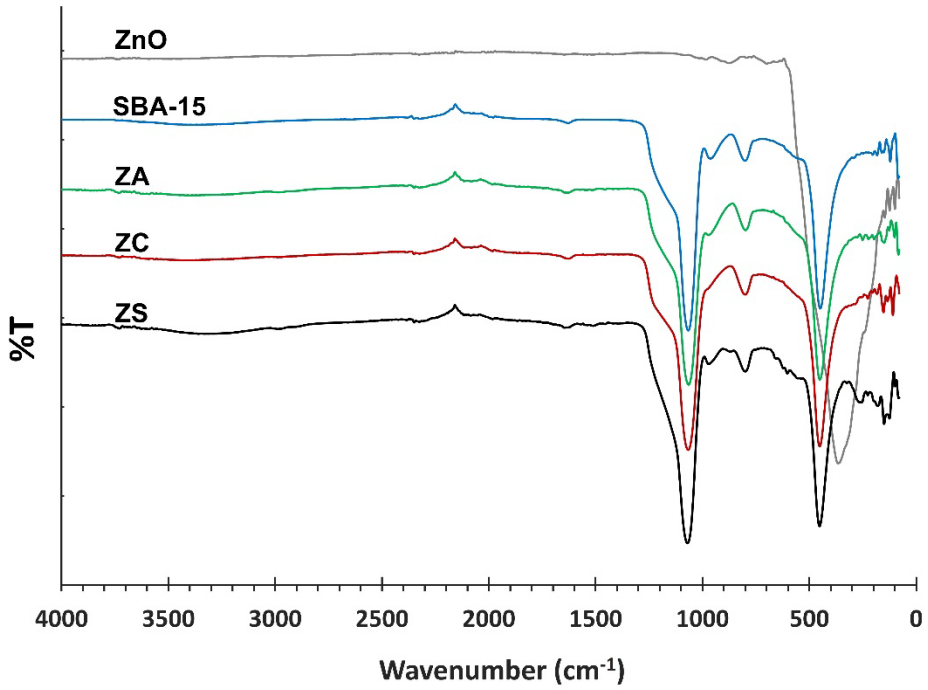

Figure 2. FTIR spectra of the commercial ZnO, SBA-15, and the catalysts.

3.1.2. The chemical state information from the surface

The XPS technique was employed to investigate the type of Zn atoms presenting on the surface of SBA-15, with their respective binding energies (BE) documented in Table 2. Intriguingly, the binding energy of Zn ($2p_{3/2}$) in all samples was observed to be higher than that of pure ZnO (1021.1–1022.0 eV) [21–24]. This discrepancy could be attributed to the interaction between the Zn atom and silica through the formation of a Si−O−Zn bond. The difference in electronegativity between Si atoms (1.90) and the Zn atom (1.65) resulted in electron withdrawal from the Zn atoms. Consequently, the reduction of electron density in the Zn atom contributes to a higher shift in its binding energy [21].

In the case of **ZA**, the Zn(2p) signal was detected at 1022.17 eV, which closely aligns with the binding energy of the pure ZnO, providing solid evidence for the presence of ZnO crystalline structures [21,25]. On the other hand, the Zn(2p) signal observed in **ZS** exhibited a higher energy value of 1023.02 eV, indicating a significant deviation of 0.88 eV from the pure ZnO. This variation could be attributed to the presence of Zn^{2+} ions with the characteristic Zn(2p) signals ranging from 1022.54 to 1023.07 eV [4,26], indicating their interaction with SBA-15. These findings further confirm the specific type of the presented Zn atoms and are consistent with the results obtained from the previous analytical techniques.

The Zn(2p) signal of **ZC** was found at 1022.71 eV, which was greater than that of **ZA**. **ZC** spectra also showed a slight signal around 200 eV, corresponding to the Zn–Cl($2p_{3/2}$) and Zn–Cl($2p_{1/2}$) species [23]. These results implied that the prepared catalysts contain ZnO and Zn^{2+} ions on the surface of the **ZC** sample. In addition, the energy difference of 23 eV between the Zn($2p_{3/2}$) and

$Zn(2p_{1/2})$ signals serves as a characteristic indicator of the presence of ZnO in both **ZA** and **ZC** samples.

Table 2. Binding energy of the Zn atom from the XPS technique.

Samples	$Zn(2p_{3/2})$	$Zn(2p_{1/2})$	Different BE
ZA	1022.17	1045.22	23.05
ZC	1022.71	1045.74	23.03
ZS	1023.02	1046.13	23.12

3.1.3. Morphological and elemental analysis

SEM and EDS analyses provided insights into the surface morphology and elemental composition of the samples, as illustrated in Figure 3 and Table 1. The surface roughness of the Zn-containing catalysts exhibited a resemblance to that of SBA-15. Notably, chlorine and sulfur atoms were detected on **ZC** and **ZS**, indicating an incomplete decomposition of $ZnCl_2$ and $ZnSO_4$ into ZnO.

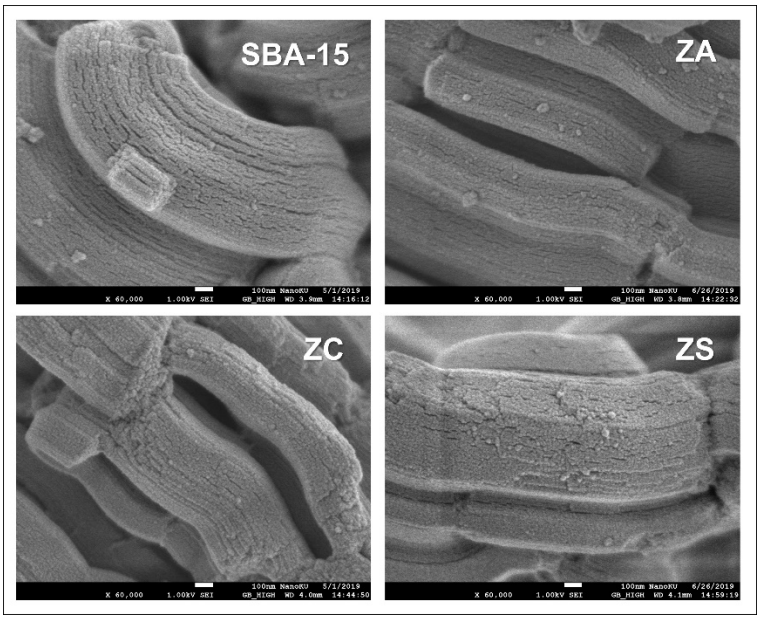

Figure 3. Surface morphology of the samples investigated by SEM.

Table 1. Atomic composition on the surface of the samples investigated by the EDS technique.

Samples	Elemental composition (Atomic%)					
	O	Si	Zn	Cl	S	others
SBA-15	80.64	19.36	-	-	-	-
ZA	76.54	20.59	2.29	-	-	0.58
ZC	77.11	18.91	2.90	1.08	-	-
ZS	77.35	16.93	1.92	-	2.37	1.43

TEM images (Figure 4) depict a remarkable two-dimensional hexagonal and honeycomb structure with long-range ordered channels, featuring a pore diameter ranging from 6 to 8 nm. Notably, the **ZA** sample showcases the presence of aggregated ZnO particles on the surface of SBA-15. Upon closer inspection, the magnified image reveals the distinct parallel lattice fringes with a width of 0.28 nm, which corresponds to the (100) crystal face. In contrast, the **ZS** sample displays lattice fringes characteristic of $ZnSO_4$, while the **ZC** sample exhibits no discernible features apart from SBA-15. These TEM findings align perfectly with the XRD data, reinforcing the consistency of the results.

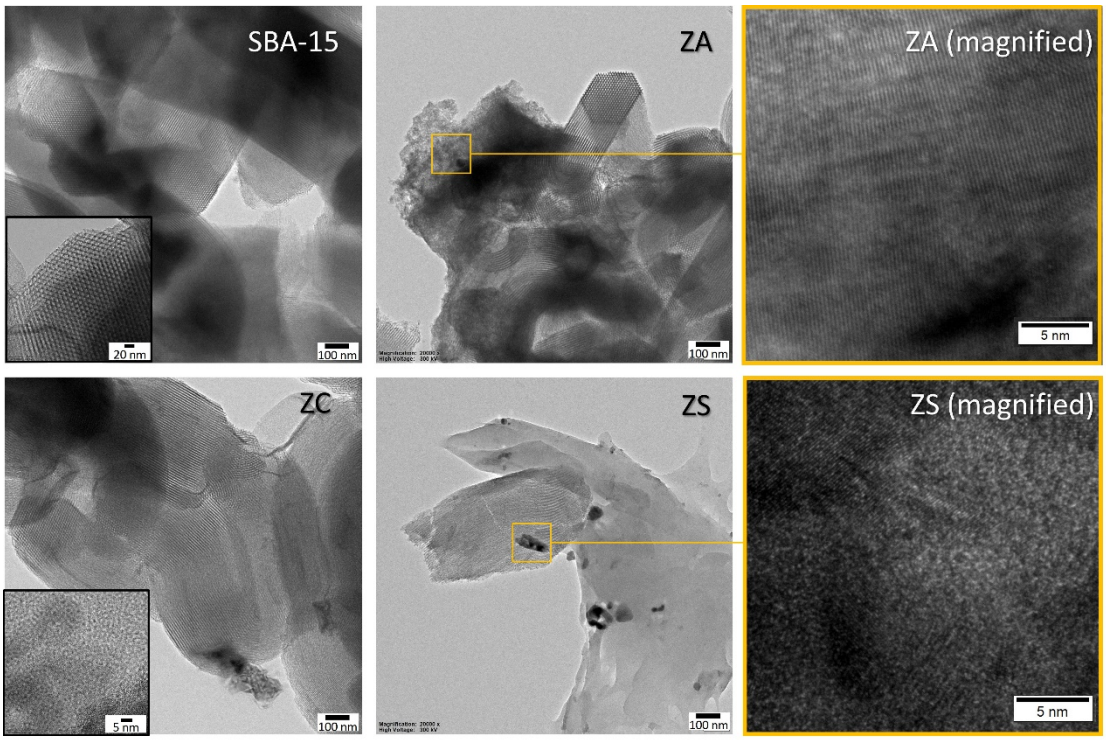

Figure 4. TEM images of SBA-15 and the catalyst samples. The scale bars of SBA-15, **ZA**, **ZC,** and **ZS** are 100 nm.

3.1.4. Surface area analysis

To assess the absorption characteristics of the sample, nitrogen adsorption/desorption isotherms were employed, providing useful insights into the surface area, pore volume, and pore size, as outlined in Table 3 . Remarkably, all isotherms exhibited Langmuir type IV adsorption behavior, while the hysteresis branches with near-parallel alignment indicated the presence of cylindrical pores with a relatively consistent pore size [27]. Notably, the Zn-containing catalysts displayed a significant reduction in both BET-specific surface area and pore volume. Interestingly, the reduction in surface area surpassed the decline in pore volume, resulting in an overall increase in pore diameter compared to the SBA-15.

Table 3. Surface area, pore volume, and pore diameter of SBA-15 and prepared catalysts.

Samples	BET Surface area (m^2/g)	BJH (Desorption)		
		Surface area (m^2/g)	Pore volume (cm^3/g)	Pore diameter* (nm)
SBA-15	651.41	550.18	0.88	6.39
ZA	333.37	390.76	0.72	7.32
ZC	291.26	346.86	0.65	7.46
ZS	289.34	304.29	0.59	7.70

*Pore diameter is calculated using BJH (desorption) as 4V/A (V = pore volume and A = surface area). The data was calculated from the raw data of surface area and pore volume with 4 and 6 decimal places, respectively.

3.1.5. Acidity of the catalysts

The acidic properties of the samples were assessed using NH_3-TPD (Figure 5). NH_3 desorption temperature indicated acid site strength: weak (T < 200 °C), moderate (200 °C < T < 500°C), and strong (T > 500°C) [28]. SBA-15 had limited acidic sites, with a broad desorption peak suggesting weak to moderate acidity. Incorporating Zn into SBA-15 increases acidic sites. **ZA** (ZnO) showed weak acidity at 160 °C and broad moderate acidity (200−400 °C) [29]. **ZS** (Zn^{2+}) exhibited a distinct desorption peak at 238 °C, indicating moderate acidity [30]. These findings align with the literature on ZnO/S-1 and Zn^{2+}/S-1 [25]. **ZC** provided the highest acidic site concentration, suggesting the coexistence of ZnO and Zn^{2+} ions. The total acidity trend is in the order of **ZC** > **ZA** > **ZS** > SBA-15.

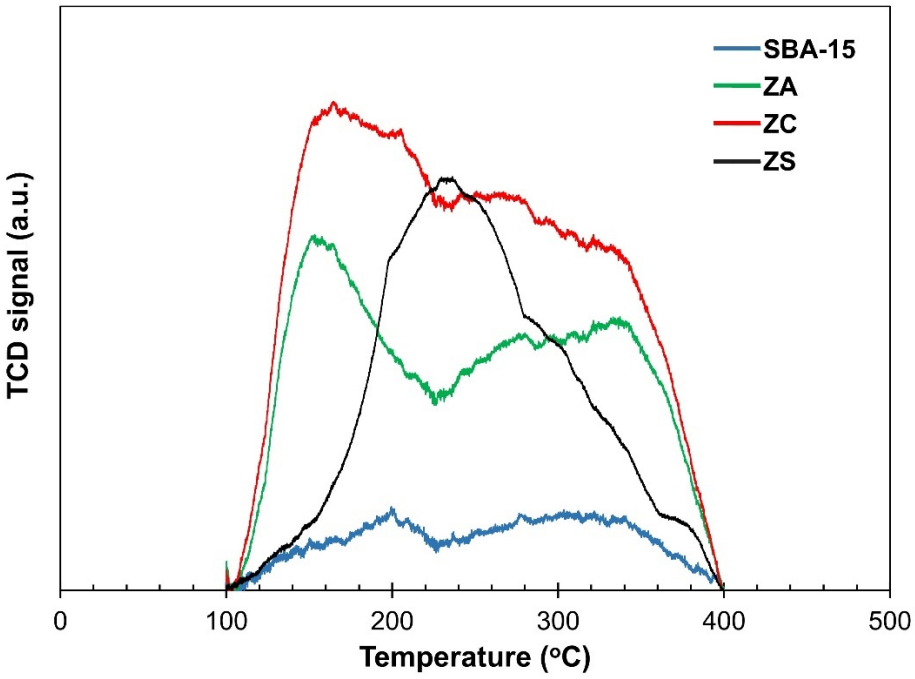

Figure 5. NH_3-TPD profiles of SBA-15 and the catalysts.

3.2. Glycolysis of PET

SBA-15 and the catalysts were tested for PET glycolysis to evaluate their efficiency in recovering the BHET monomer. The catalyst at 1% (w/w) of PET was added to the PET:EG with a 1:5 (w/w) ratio at a constant temperature of 200°C. In the presence of catalysts, the %yield of BHET ($\%Y_{BHET}$) rapidly increased within the first hour, followed by a gradual increase, and remained stabilized after 2 hours (Figure 6). Catalyst reactivity is in the order of **ZC** > **ZA** > **ZS**, which is correlated to their acidity. On the contrary to the zinc-deposited catalysts, SBA-15 exhibited no changes in the starting material after 3 hours due to the insufficiency of its acidity. Even with a small amount of Zn (1−3% atomic ratio) on the surface of SBA-15, the glycolysis reaction could be activated, yielding a higher amount of BHET compared to 15 of pure ZnO [7]. Consequently, **ZC** was selected for further optimization of PET glycolysis conditions.

The increase in catalytic efficiency can be attributed to the enhanced surface area of the active site. This suggests that the prepared catalysts exhibit a well-distributed Zn active site on the surface of SBA-15, which prevents agglomeration compared to the use of ZnO nanoparticles. Another contributing factor is the binding of Zn atoms to SBA-15, which enhances the acidity of the active site. The higher electronegativity of Si atoms compared to Zn atoms results in electron withdrawal from Zn atoms, increasing electrophilicity to accept electron pairs from carbonyl groups. Furthermore, in our research, we employed a digestion tube for PET glycolysis without additional stirring or dispersing techniques for the catalyst. During the reaction, EG vaporizes and condenses within the digestion tube. Reflux occurs when the temperature surpasses the boiling point of EG (197°C). After 2 hours, the reaction reaches equilibrium, yielding a constant BHET yield. This glycolysis method is easy to set up, employing mild reagents and requiring only an available heating source, making it suitable for potential large-scale applications.

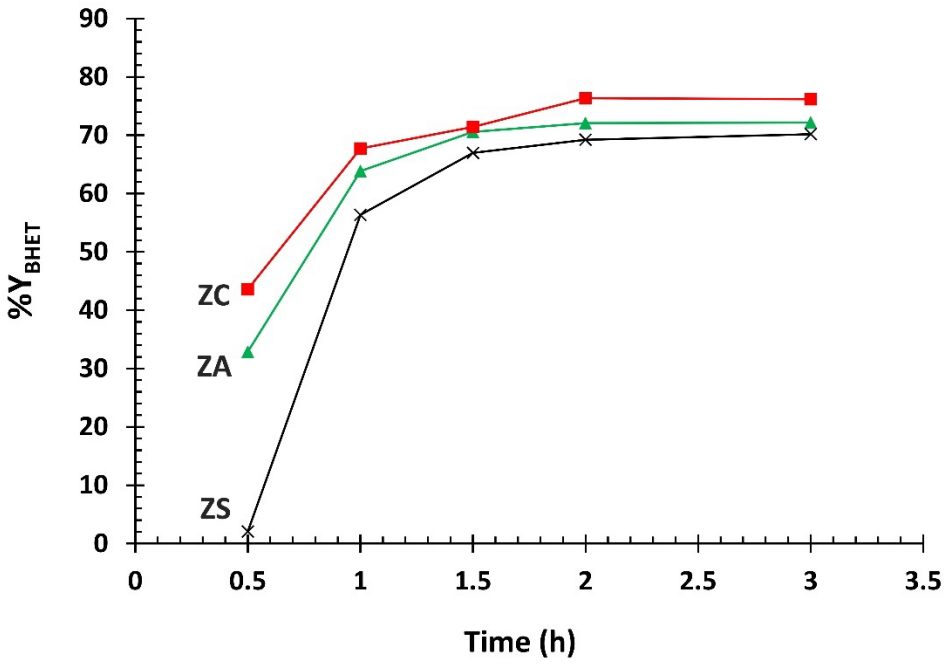

Figure 6. Efficiency of prepared catalysts on the glycolysis of PET. The reaction condition is the ratio of PET:EG (1:5) with a 1% catalyst at 200 °C.

To optimize the level of each parameter, a scanning experiment using **ZC** as the catalyst was conducted. Figure 7 illustrates that $\%Y_{BHET}$ consistently increased across all experiments. The PET:EG ratio of 1:5 was found to be adequate for the reaction, as previously reported [7]. The cost of chemical compounds was minimized by exploring the optimization range of 1:3 to 1:5. $\%Y_{BHET}$ remained constant at a temperature of 200°C and a catalyst concentration of 1%. Consequently, we conducted glycolysis experiments with 0.5−1.5% catalysts, temperatures ranging from 180−220°C, and durations of 1−2 hours, each with three replicated runs.

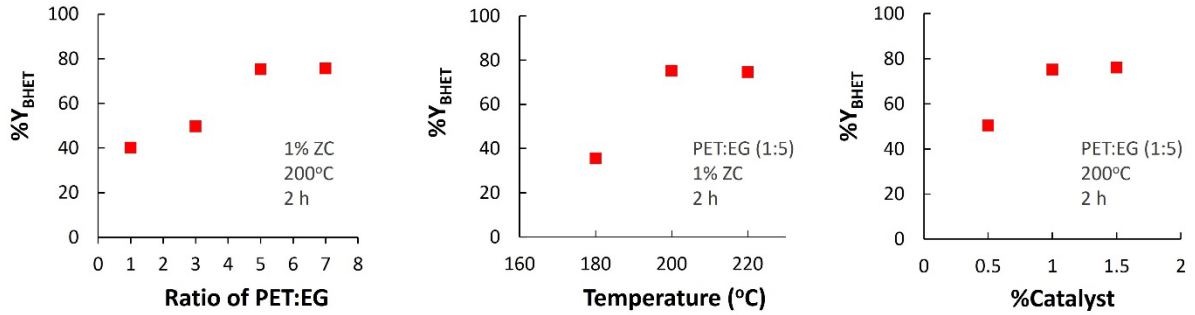

Figure 7. The scanning experiment to estimate the level of each parameter for the optimization.

Figure 8 presents the results of the optimized experiment. Temperature has a significant impact on $\%Y_{BHET}$. At a temperature of 180°C, all conditions resulted in a product yield of less than 50%, likely due to glycolysis being a diffusion-controlled kinetic reaction [31]. The softening point of PET occurs at 220°C, and it is speculated that a solvent like EG can lower this point, facilitating faster depolymerization. The reported temperature for glycolysis of PET with EG is approximately 197°C (the boiling point of EG) or higher. Increasing the EG content greatly enhances glycolysis at lower reaction temperatures, but its effectiveness diminishes at 200°C and 220°C. The addition of catalyst from 1% to 1.5% slightly improves $\%Y_{BHET}$. Glycolysis for a duration of 2 hours yields over 70% of the product, as summarized in Table 5. Based on these findings, we optimized the glycolysis conditions using a 1:5 PET:EG ratio and a 1% **ZC** catalyst at 200°C for 2 hours, resulting in a 75% yield of BHET.

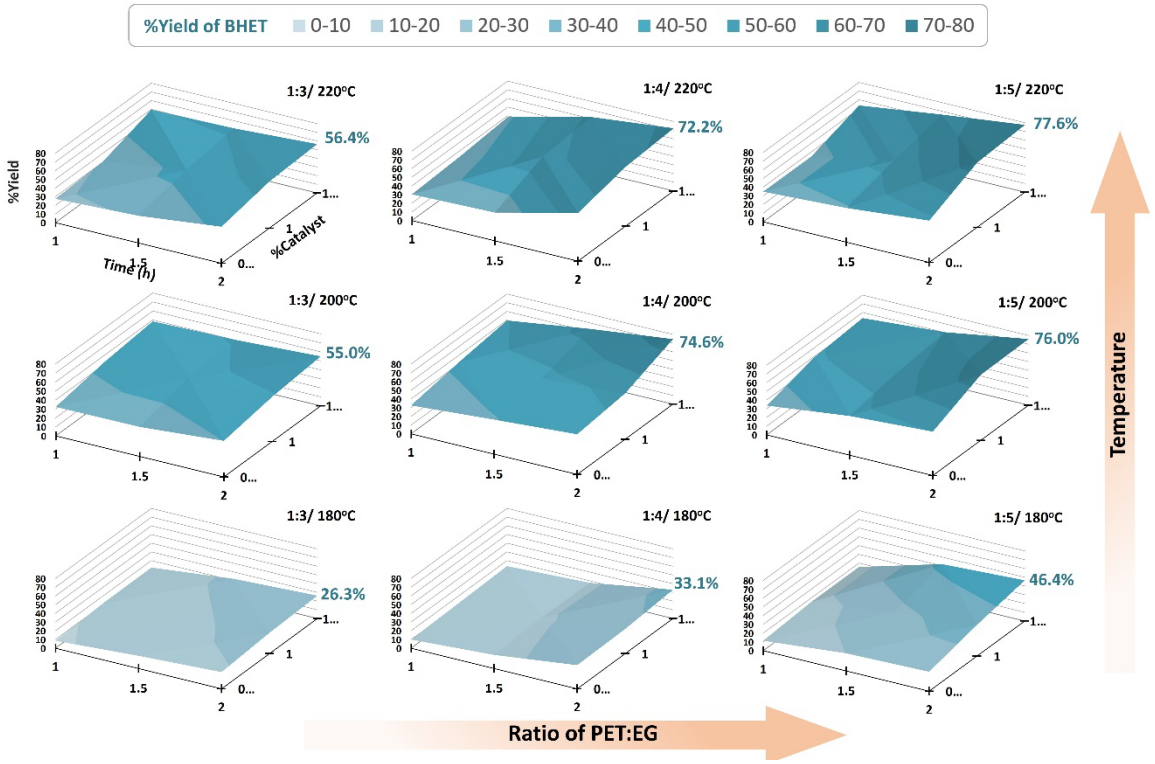

Figure 8. 3D graph for optimization of the parameters for glycolysis of PET using a **ZC** catalyst.

3.3. Purity of the BHET product

The FTIR spectrum of BHET displays prominent absorption peaks corresponding to the hydroxyl group (O−H) and carbonyl group (C=O) at wavenumbers of 3492-3432 cm^{-1} and 1713 cm^{-1}, respectively. The C−O stretching vibration signal was observed at 1270 cm^{-1}. The methylene group is identified by stretching signals at 2954−2904 cm^{-1} (C−H stretching of methylene) and a bending signal at 1408 cm^{-1} (C−H bending). The presence of the aromatic ring is confirmed by the signals at 3090 cm^{-1} (C−H stretching of unsaturated carbon), 1650−1629 cm^{-1} (C=C stretching of aromatic ring), and 730 cm^{-1} (1,4-disubstituted benzene ring), respectively. The FTIR spectrum of the obtained BHET closely resembles that of the BHET standard, confirming the purity of BHET obtained from our glycolysis reaction (see SI, Figure S1).

The purity of the BHET product was also further assessed using melting point and DSC analysis. Our product exhibited a melting point range of 107−110°C, consistent with the reported standard value [7,32]. The DSC thermogram, spanning a range of 30−200°C, displayed a single sharp endothermic peak at 111°C, with no indication of a dimer by product signal (170°C) [33]. These findings confirm the purity of the BHET obtained from the glycolysis process (see SI, Figure S2).

3.4. Reusability

The **ZC** catalyst can be recovered by filtration, followed by washing with hot distilled water and drying at 80°C for 6 hours. By recycling the catalyst three times, the producibility of the BHET remained at 70% [11,15] (see SI, Figure S3).

4. Conclusion

Impregnating SBA-15 with various zinc salts and calcining at 550°C yielded active sites in the form of ZnO and Zn^{2+} ions. The presence of Zn atoms led to a decrease in surface area and pore volume compared to bare SBA-15. XRD and XPS analysis confirmed the presence of ZnO, ZnO/Zn^{2+}, and Zn^{2+} in **ZA**, **ZC**, and **ZS**, respectively. The efficiency of catalysts in glycolysis has depended on their acidity, which is in the order of **ZC** > **ZA** > **ZS** >> SBA-15. Using a PET:EG ratio of 1:5, a 1% **ZC** catalyst based on the weight of PET, and heating at 200 °C for 2 hours resulted in the highest yield of BHET at 75% *via* recrystallization. The catalysts are conveniently prepared, reusable, and environmentally friendly. The catalyst we developed has the potential to be further enhanced in the future to enable industrial-scale PET bottle degradation. This work has implications for resource recovery and the circulation of BHET monomers in the PET industry, aligning with the goal of sustainable development.

Use of AI tools declaration

The authors declare that they have not used Artificial Intelligence (AI) tools in the creation of this article.

Acknowledgements

This work was supported in part by Kasetsart University Research and Development Institute (KURDI): R-M 26.62 and the Faculty of Science at Sriracha, Kasetsart University Sriracha campus. All are gratefully acknowledged for partial support and research facilities. Co-workers from the Faculty of Science and Technology, Suratthani Rajabhat University for supporting the chemical test equipment and laboratory area. Pailin Srisuratsiri: Data analysis, Conclusion, Recommendation, Writing-reviewing & editing. Ketsarin Chantarasunthon: Data analysis, Conclusion, Recommendation, Writing-reviewing & editing. Wanutsanun Sudsai: Investigation. Pichet Sukprasert: Investigation. Laksamee Chaicharoenwimolkul Chuaitammakit: Conceptualization, Methodology, Validation, Formal analysis, Investigation, Writing-original draft, Visualization, Supervision. Wissawat Sakulsaknimitr: Conceptualization, Methodology, Investigation, Writing-original draft, Supervision, Project administration.

Conflict of interest

The authors declare that they have no known competing financial interests or personal relationships that could have appeared to influence the work reported in this paper.

References

1. Leslie HA, van Velzen MJM, Brandsma SH, et al. (2021) Discovery and quantification of plastic particle pollution in human blood. *Environ Int* 163: 107199. https://doi.org/10.1016/j.envint.2022.107199
2. Raheem AB, Noor ZZ, Hassan A, et al. (2019) Current developments in chemical recycling of post-consumer polyethylene terephthalate wastes for new materials production: A review. *J Clean Prod*. 225: 1052–1064. https://doi.org/10.1016/j.jclepro.2019.04.019
3. Benyathiar P, Kumar P, Carpenter G, et at. (2022) Polyethylene Terephthalate (PET) Bottle-to-Bottle Recycling for the Beverage Industry: A Review. *Polymers* 14: 2366. https://doi.org/10.3390/polym14122366
4. Zhang Q, Huang R, Yao H, et al. (2021) Removal of $Zn^{2+}$from polyethylene terephthalate (PET) glycolytic monomers by sulfonic acid cation exchange resin. *J Environ Chem Eng* 9:105326. https://doi.org/10.1016/j.jece.2021.105326
5. Vieira CO, Grice JE, Roberts MS, et al. (2018) ZnO:SBA-15 nanocomposites for potential use in sunscreen: Preparation, properties, human skin penetration and toxicity. *Skin Pharmacol Physiol* 32: 32–42. https://doi.org/10.1159/000491758
6. Imran M, Kim DH, Al-Masry WA, et al. (2013) Manganese-, cobalt-, and zinc-based mixed-oxide spinels as novel catalysts for the chemical recycling of poly(ethylene terephthalate) via glycolysis. *Polym Degrad Stab*. 98: 904–915. https://doi.org/10.1016/j.polymdegradstab.2013.01.007
7. Kawkumpa S, Saisema T, Seoob O, et al. (2019) Synthesis of polyurethane from glycolysis product of PET using ZnO as catalyst. *RMUTSB Acad J* 7: 29–39 https://li01.tci-thaijo.org/index.php/rmutsb-sci/article/view/150479
8. Shen Z, Zhou H, Chen H, et al. (2018) Synthesis of Nano-Zinc Oxide Loaded on Mesoporous Silica by Coordination Effect and Its Photocatalytic Degradation Property of Methyl Orange. *Nanomater* 8: 317. https://doi.org/10.3390/nano8050317
9. Nguyen QNK, Yen NT, Hau ND, et al. (2020) Synthesis and Characterization of Mesoporous Silica SBA-15 and ZnO/SBA-15 Photocatalytic Materials from the Ash of Brickyards. *J Chem* Article ID 8456194, 8 pages: https://doi.org/10.1155/2020/8456194
10. Wen H, Zhou X, Shen Z, et al. (2019) Synthesis of ZnO nanoparticles supported on mesoporous SBA-15 with coordination effect -assist for anti-bacterial assessment. *Colloids Surf. B* 181: 285–294. https://doi.org/10.1016/j.colsurfb.2019.05.055
11. Bhuyan D, Saikia M, Saikia L. (2018) ZnO nanoparticles embedded in SBA-15 as an efficient heterogeneous catalyst for the synthesis of dihydropyrimidinones via Biginelli condensation reaction. Microporous Mesoporous Mater 256: 39–48. https://doi.org/10.1016/j.micromeso.2017.06.052
12. Pal N, Paul M, Bhaumik A. (2011) Highly ordered Zn-doped mesoporous silica: An efficient catalyst for transesterification reaction. *J Solid State Chem* 184: 1805–1812. https://doi.org/10.1016/j.jssc.2011.05.033
13. Nagvenkar A, Naik S, Fernandes J. (2015) Zinc oxide as a solid acid catalyst for esterification reaction. *Catal Commun* 65: 20–23. https://doi.org/10.1016/j.catcom.2015.02.009

14. Yao H, Liu L, Yan D, et al. (2022) Colorless BHET obtained from PET by modified mesoporous catalyst ZnO/SBA-15. *Chem Eng Sci* 248: 117109. https://doi.org/10.1016/j.ces.2021.117109
15. Datta B, Pasha MA. (2013) Silica-$ZnCl_2$: An Efficient Catalyst for the Synthesis of 4-Methylcoumarins. *ISRN Org Chem* 13: 1–5. https://doi.org/10.1155/2013/132794
16. Lin CC, Li YY. (2009) Synthesis of ZnO nanowires by thermal decomposition of zinc acetate dihydrate. *Mater Chem Phys* 113: 334–337. https://doi.org/10.1016/j.matchemphys.2008.07.070
17. Jones F, Tran H, Lindberg D, et al. (2013) Thermal Stability of Zinc Compounds. *Energy and Fuels* 27: 5663–5669. https://doi.org/10.1021/ef400505u
18. Moosavi A, Sarrafi M, Aghaei A, et al. (2012) Synthesis of mesoporous ZnO/SBA-15 composite via sonochemical route. *Micro Nano Lett* 7: 130–133. DOI:10.1049/mnl.2011.0461
19. Saha J, Podder J. (2011) Crystallization Of Zinc Sulphate Single Crystals And Its Structural, Thermal And Optical Characterization. *J Bangladesh Acad Sci* 35: 203–210. https://doi.org/10.3329/jbas.v35i2.9426
20. Foad Raji MP. (2013) Study of Hg(II) species removal from aqueous solution using hybrid $ZnCl_2$-MCM-41 adsorbent. *Appl Surf Sci* 282: 415–424. https://doi.org/10.1016/j.apsusc.2013.05.145
21. Jiang Q, Wu ZY, Wang YM, et al. (2006) Fabrication of photoluminescent ZnO/SBA-15 through directly dispersing zinc nitrate into the as-prepared mesoporous silica occluded with template. *J Mater Chem* 16: 1536–1542. https://doi.org/10.1039/B516061H
22. Tay YY, Li S, Sun CQ, et al. (2006) Size dependence of Zn 2p 32 binding energy in nanocrystalline ZnO. *Appl Phys Lett* 88: 173118. https://doi.org/10.1063/1.2198821
23. Winiarski J, Tylus W, Winiarska K, et al. (2018) XPS and FT-IR Characterization of Selected Synthetic Corrosion Products of Zinc Expected in Neutral Environment Containing Chloride Ions. *J Spectrosc* Article ID 2079278. https://doi.org/10.1155/2018/2079278
24. Miyao T, Kitai M, Ogita T, et al. (2002) Generation of new acidic sites by dispersing zinc oxide fine particles on silica. *Zeitschrift fur Phys Chemie* 216: 931–939. https://doi.org/10.1524/zpch.2002.216.7.931
25. Gabrienko AA, Arzumanov SS, Toktarev AV, et al. (2017) Different Efficiency of Zn^{2+} and ZnO Species for Methane Activation on Zn-Modified Zeolite. *ACS Catal* 7: 1818–1830. https://doi.org/10.1021/acscatal.6b03036
26. Zhiyong Y, Bensimon M, Sarria V, et al. (2007) $ZnSO_4$-TiO_2 doped catalyst with higher activity in photocatalytic processes. *Appl Catal B Environ* 76: 185–195. https://doi.org/10.1016/j.apcatb.2007.05.025
27. Cychosz KA, Thommes M. (2018) Progress in the Physisorption Characterization of Nanoporous Gas Storage *Materials. Engineering*. 4: 559–566. https://doi.org/10.1016/j.eng.2018.06.001
28. Lao-Ubol S, Khunlad R, Larpkiattaworn S, et al. (2016) Preparation, Characterization and Catalytic Performance of ZnO-SBA-15 Catalysts. *Key Eng Mater* 690: 212–217. https://doi.org/10.4028/www.scientific.net/KEM.690.212

29. Liu J, Liu Y, Liu H, et al. (2021) Silicalite-1 Supported ZnO as an Efficient Catalyst for Direct Propane Dehydrogenation. *ChemCatChem* 13: 4780–4786. https://doi.org/10.1002/cctc.202101069
30. Liu G, Liu J, He N, Miao C, et al. (2018) Silicalite-1 zeolite acidification by zinc modification and its catalytic properties for isobutane conversion. *RSC Adv* 8: 18663–18671. https://doi.org/10.1039/C8RA02467G
31. Xin J, Zhang Q, Huang J, et al. (2021) Progress in the catalytic glycolysis of polyethylene terephthalate. *J Environ Manage*. 296: 113267. https://doi.org/10.1016/j.jenvman.2021.113267
32. Al-Sabagh AM, Yehia FZ, Eshaq G, et al. (2016) Greener routes for recycling of polyethylene terephthalate. *Egypt J Pet* 25: 53–64. https://doi.org/10.1016/j.ejpe.2015.03.001
33. Imran M, Kim BK, Han M, et al. (2010) Sub- and supercritical glycolysis of polyethylene terephthalate (PET) into the monomer bis(2-hydroxyethyl) terephthalate (BHET). *Polym Degrad Stab* 95:1686–1693. https://doi.org/10.1016/j.polymdegradstab.2010.05.026

AIMS Press